In-medium $NN \to N\Delta$ cross section and its dependence on effective Lagrange parameters in isospin-asymmetric nuclear matter*

Ying Cui(崔莹)[1;1)] Ying-Xun Zhang(张英逊)[1,2;2)] Zhu-Xia Li(李祝霞)[1]

[1]China Institute of Atomic Energy, Beijing 102413, China
[2]Guangxi Key Laboratory Breeding Base of Nuclear Physics and Technology, Guangxi Normal University, Guilin 541004, China

Abstract: The in-medium $NN \to N\Delta$ cross sections and its differential cross sections in isospin asymmetric nuclear medium are investigated in the framework of the one-boson exchange model by including isovector mesons, i.e., δ and ρ mesons. Our results show that the in-medium $NN \to N\Delta$ cross sections are suppressed when the density increases, and the differential cross sections become isotropic with an increase in the density around the Δ threshold energy. The isospin splitting on the medium correction factor, $R = \sigma^*_{NN\to N\Delta}/\sigma^{\rm free}_{NN\to N\Delta}$ is observed for different channels of $NN \to N\Delta$, especially around the threshold energy for all the effective Lagrangian parameters. By analyzing the selected effective Lagrangian parameters, our results show that the larger effective mass is, the weaker medium correction R is.

Keywords: in-medium $NN \to N\Delta$ cross section, isospin-asymmetric nuclear matter, Lagrangian parameters, differential cross section

PACS: 24.10. Cn, 25.70.-z **DOI:** 10.1088/1674-1137/43/2/024105

1 Introduction

The isospin dependence of in-medium NN cross sections is a subject of much interest in the field of intermediate energy neutron-rich heavy ion collisions (HIC), because it can influence the predictions of reaction dynamics, collective flow, stopping power, and particle productions in HIC simulations [1-8]. By comparing the HIC experimental data to the transport model calculations, information on in-medium NN cross section and equation of state (EOS) can be indirectly extracted. Principally, both the mean field (or EOS) and nucleon-nucleon cross sections in the transport models should be determined by the same effective Lagrangian or effective interaction. However, the mean field potential and nucleon-nucleon cross section in different transport models are treated independently, owing to the complexity of the transport equations and, particularly, their dimensionality. In particular, the solution of the collision integral is not obtained directly but through the Monte-Carlo cascade method, in which the in-medium nucleon-nucleon scattering cross sections are adopted, and their correction factor is ad hoc determined by fitting the related HIC observables. Thus, the direction of further improving the transport models in theory is to consider the mean field and nucleon-nucleon cross section consistently, it naturally requires to understand the relation between the in-medium NN cross section and the EOS (or the nuclear matter parameters).

Several studies have investigated the in-medium NN elastic cross section and its isospin dependence using microscopic approaches [9-12]. In transport models, the isospin-dependent medium correction factor $R = \dfrac{\sigma^*}{\sigma^{\rm free}} = \left(\dfrac{m^*}{m}\right)^2$ for elastic NN cross sections was adopted in the isospin-dependent Boltzmann-Uhling-Uhlenbeck and Lanzhou quantum molecular dynamics [13-15] models. In addition, phenomenological forms have also been applied to different versions of quantum molecular dynamics models (ImQMD, UrQMD), such as $R = (1-\alpha\rho/\rho_0)$ [16], $R = F(\rho, p)$ [8, 17], and $\sigma^* = \sigma_0 \tanh(\sigma^{\rm free}/\sigma_0)$ in Boltzmann-Uhling-Uhlenbeck models (pBUU) [18]. However, few theoretical works discuss the relation between the in-medium $NN \to N\Delta$ cross section and the

Received 9 November 2018, Published online 14 January 2019

* Supported by National Natural Science Foundation of China (11875323, 11875125, 11475262, 11365004, 11375062, 11790323, 11790324, 11790325) and the National Key R&D Program of China (2018 YFA0404404)

1) E-mail: yingcuid@163.com
2) E-mail: zhyx@ciae.ac.cn

EOS parameters, which has become increasingly important for further development of the transport models to study the physics around the Δ threshold energy. Especially, with the urgent requirements on constraints of symmetry energy at supersaturation density.

Recently, the isospin-dependent elementary two-body $NN \to N\Delta$ cross section, i.e., $\tilde{\sigma}^*_{NN\to N\Delta}$, was studied in the framework of relativistic Boltzmann-Uehling-Uhlenbeck microscopic transport theory by Li and Li [19]. Their results showed that the $\tilde{\sigma}^*_{NN\to N\Delta}$ has a sharp increase around the threshold energy, without considering the Δ mass distribution, and the medium correction factor $R = \tilde{\sigma}^*_{NN\to N\Delta}/\sigma^{\rm free}_{NN\to N\Delta}$ clearly depends on the isospin channels of $NN \to N\Delta$, i.e., $pp \to n\Delta^{++}$, $pp \to p\Delta^{+}$, $pn \to n\Delta^{+}$, $pn \to p\Delta^{0}$, $nn \to n\Delta^{0}$, and $nn \to p\Delta^{-}$, in isospin asymmetric nuclear matter. As a short-living resonance, Δ subsequently decays into a nucleon and a pion, and the measured cross section for $NN \to N\Delta$ is the elementary two-body cross section averaged over the mass distribution of Δ resonance. Thus, the medium correction factor R, including the effects from the mass distribution of Δ, should be investigated. Furthermore, the scalar and vector self-energies of the incoming and outgoing particles are different in the $NN \to N\Delta$ process in isospin asymmetric nuclear matter, which named as threshold energy effects in Δ production [20-22]. In our previous work [23], this effect on the in-medium $NN \to N\Delta$ cross section was analyzed. Our results confirm the isospin splitting of R near the threshold energy in isospin asymmetric nuclear matter; however, the splitting magnitude tends to vanish when the beam energy is above 1.0 GeV.

We studied in-medium $NN \to N\Delta$ cross sections and their differential cross sections under the three effective Lagrangian parameters in the isospin asymmetric nuclear matter, i.e., NL$\rho\delta$, DDMEδ, and DDRH$\rho\delta$ to further understand the relation between the in-medium $NN \to N\Delta$ cross section and the nuclear matter parameters. The effective Lagrangian and the model of the in-medium $NN \to N\Delta$ cross section are briefly described in Section 2. In Section 3, we discuss the results of isospin-dependent in-medium $NN \to N\Delta$ cross sections in different effective Lagrangian and analyze its relation to the effective mass. In addition, we briefly discuss its dependence on the slope of symmetry energy in the theoretical framework used in this study. A summary is provided in Section 4.

2 The model

2.1 Effective Lagrangian and nuclear matter properties

To calculate the in-medium $NN \to N\Delta$ cross sections in isospin asymmetric nuclear matter, we used the one-boson exchange model with the relativistic Lagrangian including nucleon and Δ (Δ is the Rarita-Schwinger spinor of spin-3/2 [24-26]), which are coupled to σ, ω, ρ, δ, and π mesons. Unlike the work in Ref. [27], we included the isovector mesons ρ and δ to describe the isospin asymmetric nuclear matter and isospin-dependent in-medium $NN \to N\Delta$ cross section. The Lagrangian we used is as follows:

$$\mathcal{L} = \mathcal{L}_I + \mathcal{L}_F, \tag{1}$$

where $\mathcal{L}_F$ is

$$\begin{aligned}\mathcal{L}_F =& \bar{\Psi}[i\gamma_\mu\partial^\mu - m_N]\Psi + \bar{\Delta}_\lambda[i\gamma_\mu\partial^\mu - m_\Delta]\Delta^\lambda \\ &+ \frac{1}{2}\left(\partial_\mu\sigma\partial^\mu\sigma - m_\sigma^2\sigma^2\right) - U(\sigma) \\ &- \frac{1}{4}\omega_{\mu\nu}\omega^{\mu\nu} + \frac{1}{2}m_\omega^2\omega_\mu\omega^\mu \\ &+ \frac{1}{2}\left(\partial_\mu\boldsymbol{\pi}\partial^\mu\boldsymbol{\pi} - m_\pi^2\boldsymbol{\pi}^2\right) - \frac{1}{4}\boldsymbol{\rho}_{\mu\nu}\boldsymbol{\rho}^{\mu\nu} + \frac{1}{2}m_\rho^2\boldsymbol{\rho}_\mu\boldsymbol{\rho}^\mu \\ &+ \frac{1}{2}\left(\partial_\mu\boldsymbol{\delta}\partial^\mu\boldsymbol{\delta} - m_\delta^2\boldsymbol{\delta}^2\right),\end{aligned} \tag{2}$$

$U(\sigma)$ is the nonlinear potential of σ field,

$$U(\sigma) = \begin{cases} \frac{1}{3}g_2\sigma^3 + \frac{1}{4}g_3\sigma^4 & \text{NL}\rho\delta \\ 0 & \text{DDME}\delta, \text{DDRH}\rho\delta \end{cases} \tag{3}$$

$\mathcal{L}_I$ is

$$\begin{aligned}\mathcal{L}_I =& \mathcal{L}_{NN} + \mathcal{L}_{\Delta\Delta} + \mathcal{L}_{N\Delta} \\ =& \Gamma_{\sigma NN}\bar{\Psi}\Psi\sigma - \Gamma_{\omega NN}\bar{\Psi}\gamma_\mu\Psi\omega^\mu - \Gamma_{\rho NN}\bar{\Psi}\gamma_\mu\boldsymbol{\tau}\cdot\Psi\boldsymbol{\rho}^\mu \\ &+ \frac{g_{\pi NN}}{m_\pi}\bar{\Psi}\gamma_\mu\gamma_5\boldsymbol{\tau}\cdot\Psi\partial^\mu\boldsymbol{\pi} + \Gamma_{\delta NN}\bar{\Psi}\boldsymbol{\tau}\cdot\Psi\boldsymbol{\delta} \\ &+ \Gamma_{\sigma\Delta\Delta}\bar{\Delta}_\mu\Delta^\mu\sigma - \Gamma_{\omega\Delta\Delta}\bar{\Delta}_\mu\gamma_\nu\Delta^\mu\omega^\nu \\ &- \Gamma_{\rho\Delta\Delta}\bar{\Delta}_\mu\gamma_\nu\boldsymbol{T}\cdot\Delta^\mu\boldsymbol{\rho}^\nu + \frac{g_{\pi\Delta\Delta}}{m_\pi}\bar{\Delta}_\mu\gamma_\nu\gamma_5\boldsymbol{T}\cdot\Delta^\mu\partial^\nu\boldsymbol{\pi} \\ &+ \Gamma_{\delta\Delta\Delta}\bar{\Delta}_\mu\boldsymbol{T}\cdot\Delta^\mu\boldsymbol{\delta} + \frac{g_{\pi N\Delta}}{m_\pi}\bar{\Delta}_\mu\mathcal{T}\cdot\Psi\partial^\mu\boldsymbol{\pi} \\ &+ \frac{ig_{\rho N\Delta}}{m_\rho}\bar{\Delta}_\mu\gamma_\nu\gamma_5\mathcal{T}\cdot\Psi(\partial^\nu\boldsymbol{\rho}^\mu - \partial^\mu\boldsymbol{\rho}^\nu) + h.c.\end{aligned} \tag{4}$$

$\omega_{\mu\nu}$ and $\boldsymbol{\rho}_{\mu\nu}$ in Eq. (2) are defined by $\partial_\mu\omega_\nu - \partial_\nu\omega_\mu$ and $\partial_\mu\boldsymbol{\rho}_\nu - \partial_\nu\boldsymbol{\rho}_\mu$, respectively. Here, $\boldsymbol{\tau}$ and $\boldsymbol{T}$ are the isospin matrices of the nucleon and Δ [25, 26], and $\mathcal{T}$ is the isospin transition matrix between the isospin 1/2 and the 3/2 fields [24]. Γ_{mNN} is the meson-nucleon coupling constant

$$\Gamma_{mNN} = \begin{cases} g_{mNN} & \text{NL}\rho\delta \\ g_{mNN}(\rho_B) & \text{DDME}\delta, \text{DDRH}\rho\delta \end{cases} \tag{5}$$

The values of Γ_{mNN} are listed in Table 1.

For the coupling constants $\Gamma_{m\Delta\Delta}$, $m = \sigma, \omega, \rho, \delta$, we simply take them to be equal to the meson-nucleon-nucleon coupling, i.e., $\Gamma_{m\Delta\Delta} = \Gamma_{mNN}$, similar to the transport model calculations [19, 20, 27]. The coupling constant $g_{\pi N\Delta}$ must be calculated for describing the $NN \to N\Delta$ cross section, and it is determined by analyzing the Δ-isobar decay width from Ref. [28]. However, the π meson in the relativistic mean field does not contribute to the

Table 1. Parameters used in the effective Lagrangian, $g_{\pi NN}$=1.008, $g_{\pi N\Delta}$=2.202, m_π=138, m_N=939, $m_{0,\Delta}$=1232 (all masses are in MeV), $g_2/g^3_{\sigma NN}$=0.03302 fm^{-1} (NL$\rho\delta$), $g_3/g^4_{\sigma NN}$=−0.00483 (NL$\rho\delta$), $\Lambda_{\pi NN}$=1000 MeV. The coupling constants Γ_{mNN} and $g_{mN\Delta}$ are dimensionless.

	NL$\rho\delta$-Δ	DDMEδ-Δ[a]	DDRH$\rho\delta$-Δ[a]
m_σ/MeV	550	566	550
m_ω/MeV	783	783	783
m_ρ/MeV	770	769	763
m_δ/MeV	980	983	980
$\Gamma_{\sigma NN}$	8.9679	10.3313	10.7286
$\Gamma_{\omega NN}$	9.2408	12.2905	13.2902
$\Gamma_{\rho NN}$	6.9256	6.3117	5.8284
$\Gamma_{\delta NN}$	7.8525	7.1515	7.6009
$\Lambda_{\pi N\Delta}$/MeV	410	416	417
$\Lambda_{\rho NN}$/MeV	1000	650	580
E/A/MeV	−16.00	−16.12	−16.25
ρ_0/fm^{-3}	0.160	0.152	0.153
K_0/ MeV	240.0	219.1	240.2
S_0/MeV	30.60	32.35	25.34
L/MeV	101.46	52.85	45.33
m^*_N/m_N	0.75	0.609	0.55
m^*_Δ/m_Δ	0.809	0.702	0.661
Δm^{*}_N[b]	0.0312	0.0236	0.0265
Δm^{*}_Δ[b]	0.0079	0.0060	0.0068

[a]The values of coupling constants at $\rho_B=\rho_0$ for DDMEδ-Δ and DDRH$\rho\delta$-Δ. [b]Here $\Delta m^*_N=\frac{m^*_p-m^*_n}{m_N}$ and $\Delta m^*_\Delta=\frac{m^*_{\Delta^{++}}-m^*_{\Delta^-}}{m_\Delta}$.

EOS without the Fock term. For the coupling constant $g_{\rho N\Delta}$, we use $g_{\rho N\Delta}\approx\frac{\sqrt{3}}{2}\Gamma_{\rho NN}\frac{m_\rho}{m_N}$, which is derived using the static quark model [24, 29].

The coupling constants of nucleon to σ, ω, ρ, and δ mesons are important for the prediction of the in-medium $NN\to N\Delta$ cross section, as well as for the EOS. In this work, we selected three parameter sets, i.e., NL$\rho\delta$, DDMEδ, and DDRH$\rho\delta$ from five alternative sets [30-34], which contain σ, ω, ρ, and δ, and the compressibility was in a reasonable region, i.e., $K_0=230\pm40$ MeV as in [35]. For the NL$\rho\delta$ parameter set, $U(\sigma)$ includes the nonlinear σ self-interaction, which can reproduce reasonable values of the incompressibility and nucleon effective mass by adding two additional free parameters; however, it can also be realized by adopting the density-dependent coupling constants in DDMEδ [34] and DDRH$\rho\delta$ [32]. Because we included Δ degree in the effective Lagrangian, we labeled them as NL$\rho\delta$-Δ, DDMEδ-Δ, and DDRH$\rho\delta$-Δ in this paper to distinguish them from the original parameter sets in the relativistic mean field model (RMF).

In the nuclear matter at rest, the effective momentum can be written as $\boldsymbol{p}^*_i=\boldsymbol{p}_i$ because the spatial components of the vector field vanish, i.e., $\boldsymbol{\Sigma}=0$. Thus, in the mean field approach, the effective energy is

$$p^{*0}_i=p^0_i-\Sigma^0_i, \tag{6}$$

and

$$\Sigma^0_i=\Gamma_{\omega NN}\bar{\omega}^0+\Gamma_{\rho NN}t_{3,i}\bar{\rho}^0_3. \tag{7}$$

Here, $t_{3,i}$ is the third component of the isospin of the nucleon and Δ, and i = n, p, Δ^{++}, Δ^+, Δ^0, Δ^-, where $t_{3,n}=-1$, $t_{3,p}=1$, $t_{3,\Delta^{++}}=1$, $t_{3,\Delta^+}=\frac{1}{3}$, $t_{3,\Delta^0}=-\frac{1}{3}$, $t_{3,\Delta^-}=-1$, and $\bar{\rho}^0_3=\frac{\Gamma_{\rho NN}}{m^2_\rho}(\rho_p-\rho_n)$. The Dirac effective masses of nucleon and Δ are

$$m^*_i=m_i+\Sigma^S_i, \tag{8}$$

where

$$\Sigma^S_i=-\Gamma_{\sigma NN}\bar{\sigma}-\Gamma_{\delta NN}t_{3,i}\bar{\delta}_3, \tag{9}$$

and $\bar{\delta}_3=\frac{\Gamma_{\delta NN}}{m^2_\delta}(\rho^S_p-\rho^S_n)$.

The density-dependent of symmetry energy is

$$S(\rho_B)=\frac{k^2_F}{6E^*_F}+\frac{\Gamma^2_{\rho NN}}{2m^2_\rho}\rho_B -\frac{1}{2}\frac{\Gamma^2_{\delta NN}}{m^2_\delta}\frac{m^{*2}_N\rho_B}{E^{*2}_F\left(1+\frac{\Gamma^2_{\delta NN}}{m^2_\delta}A(k_F,m^*_N)\right)}, \tag{10}$$

which depends on the effective mass, coupling constant of $\Gamma_{\rho NN}$, and $\Gamma_{\delta NN}$. The slope of symmetry energy L is:

$$L=3\rho_0\frac{\mathrm{d}S(\rho_B)}{\mathrm{d}\rho_B}|_{\rho_B=\rho_0}=L^{\mathrm{kin}}+L^\rho+L^\delta, \tag{11}$$

where

$$L^{\mathrm{kin}}=\frac{k^2_F}{6E^*_F}\left(2-\frac{k^2_F}{E^{*2}_F}-\frac{3m^{*2}_N}{E^{*2}_F}\frac{\rho_0}{m^*_N}\frac{\partial m^*_N}{\partial\rho_B}\right) \tag{12}$$

$$L^\rho=\frac{\Gamma^2_{\rho NN}}{2m^2_\rho}\rho_0\left(3+6\frac{\rho_0}{\Gamma_{\rho NN}}\frac{\partial\Gamma_{\rho NN}}{\partial\rho_B}\right) \tag{13}$$

$$\begin{aligned}L^\delta=&-\frac{1}{2}\frac{\Gamma^2_{\delta NN}}{m^2_\delta}\frac{m^{*2}_N\rho_0}{E^{*2}_F\left(1+\left(\frac{\Gamma_{\delta NN}}{m_\delta}\right)^2A\right)}\times\left\{3+6\frac{\rho_0}{\Gamma_{\delta NN}}\frac{\partial\Gamma_{\delta NN}}{\partial\rho_B}\right.\\&-\frac{2k^2_F}{E^{*2}_F}+6\left(1-\frac{m^{*2}_N}{E^{*2}_F}\right)\frac{\rho_0}{m^*_N}\frac{\partial m^*_N}{\partial\rho_B}-3\frac{\Gamma^2_{\delta NN}}{m^2_\delta}\frac{1}{1+\frac{\Gamma^2_{\delta NN}}{m^2_\delta}A}\\&\times\left[2A\left(\frac{\rho_0}{\Gamma_{\delta NN}}\frac{\partial\Gamma_{\delta NN}}{\partial\rho_B}+\frac{\rho_0}{m^*_N}\frac{\partial m^*_N}{\partial\rho_B}\right)\right.\\&\left.\left.+\rho_0\frac{k^2_F}{E^{*3}_F}\left(1-3\frac{\rho_0}{m^*_N}\frac{\partial m^*_N}{\partial\rho_B}\right)\right]\right\},\end{aligned} \tag{14}$$

with $E_F^* = \sqrt{k_F^2 + m_N^{*2}}$ and

$$A = \frac{2}{\pi^2}\int_0^{k_F} \frac{k^4 \mathrm{d}k}{\left(k^2 + m_N^{*2}\right)^{3/2}}. \quad (15)$$

The corresponding nuclear matter parameters at normal density are listed in the lower part of Table 1, where the NL$\rho\delta$-Δ predicts the largest slope of symmetry energy L, effective mass m^*, effective mass splitting $\Delta m_N^* = (m_p^* - m_n^*)/m_N$, and $\Delta m_\Delta^* = (m_{\Delta^{++}}^* - m_{\Delta^+}^*)/m_\Delta$, among these three parameter sets at normal density. For the symmetry energy coefficient S_0, the DDRH$\rho\delta$-Δ predicts the smallest value and DDMEδ-Δ predicts the largest value among the three selected parameter sets. Among the three selected parameter sets, the larger L corresponds to larger m^*.

In Fig. 1, we present the Dirac effective masses as functions of density for nucleon and Δ in symmetric nuclear matter. The black solid lines, red dashed, and green dotted lines denote the results for NL$\rho\delta$-Δ, DDMEδ-Δ, and DDRH$\rho\delta$-Δ, respectively. The upper panel is the effective masses for nucleons and the middle panel is the effective Δ pole masses. Among the selected parameter sets, NL$\rho\delta$-Δ has the largest effective mass, while DDRH$\rho\delta$-Δ has the smallest value. In symmetric nuclear matter, m_N^*/m_N=0.75, m_N^*/m_N=0.609, and m_N^*/m_N=0.55 for NL$\rho\delta$-Δ, DDMEδ-Δ, and DDRH$\rho\delta$-Δ at saturation density, respectively. In the neutron-rich matter, the effective masses of nucleons and Δ are split owing to the contributions from the isovector-scalar δ meson. There is $m_p^* > m_n^*$, $m_{0,\Delta^{++}}^* > m_{0,\Delta^+}^* > m_{0,\Delta^0}^* > m_{0,\Delta^-}^*$. The splitting magnitude of the effective masses for nucleons and Δ depends on the coupling constant $\Gamma_{\delta NN}(\Gamma_{\delta\Delta\Delta})$ and $\bar{\delta}_3$ in Eq. (9). Here, we define the splitting magnitude of the effective mass as $\Delta m_N^*/m_N = (m_p^* - m_n^*)/m$ and $\Delta m_\Delta^*/m_\Delta = (m_{\Delta^{++}}^* - m_{\Delta^+}^*)/m_\Delta$. As shown in the bottom panel of Fig. 1, NL$\rho\delta$-Δ gives the largest effective mass splitting above normal density, but the two other parameter sets DDMEδ-Δ and DDRH$\rho\delta$-Δ predict a comparatively small effective mass splitting because the strength of $\Gamma_{\delta NN}(\Gamma_{\delta\Delta\Delta})$ decreases with density.

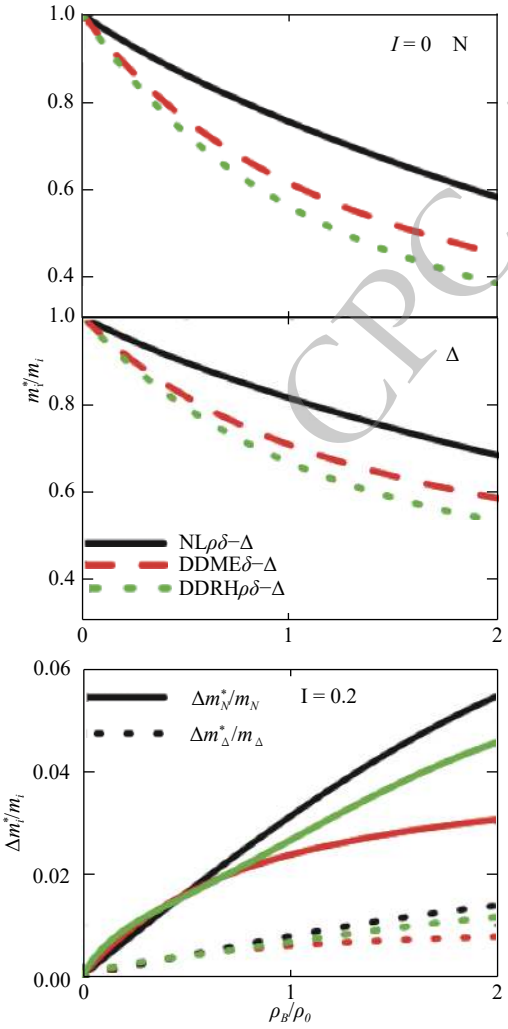

Fig. 1. (color online) (a) and (b) Effective masses of nucleon and effective pole masses of Δ as a function of ρ_B/ρ_0 in symmetric nuclear matter. (c) Effective masses splitting as a function of density for nucleons and Δs at I=0.2.

2.2 In-medium $NN \to N\Delta$ cross section

In quasiparticle approximation [36], the in-medium cross sections are introduced by replacing the vacuum plane waves of the initial and final particles with the plane waves obtained by the solution of the nucleon and Δ equation of motion with scalar and vector fields. In detail, the matrix elements $\mathcal{M}^*$ for the inelastic scattering process $NN \to N\Delta$ are obtained by replacing the nucleon and Δ masses and momenta in free space with their effective masses and kinetic momenta [27], i.e., $m \to m^*$ and $p^\mu \to p^{*\mu}$. In this work, all the calculations were performed in the center-of-mass frame of colliding particles, it coincides with the nuclear matter rest frame, where the spatial components of the vector field vanish [27].

The Feynmann diagrams corresponding to the inelastic-scattering $NN \to N\Delta$ processes are shown in Fig. 2, which include the direct and exchange processes. The $\mathcal{M}^*$-matrix for the interaction Lagrangian Eq. (4) can be written by the standard procedure [24],

$$\mathcal{M}^* = \mathcal{M}_d^{*\pi} - \mathcal{M}_e^{*\pi} + \mathcal{M}_d^{*\rho} - \mathcal{M}_e^{*\rho}, \quad (16)$$

where

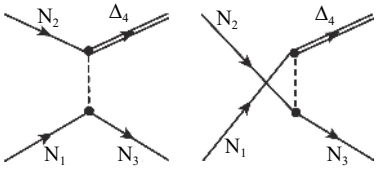

Fig. 2. Left diagram represents the direct term; right diagram represents the exchange term.

$$\mathcal{M}_d^{*\pi} = -i\frac{g_{\pi NN}g_{\pi N\Delta}I_d}{m_\pi^2(Q_d^{*2}-m_\pi^2)}[\bar{\Psi}(p_3^*)\gamma_\mu\gamma_5 Q_d^{*\mu}\Psi(p_1^*)] \times[\bar{\Delta}_\nu(p_4^*)Q_d^{*\nu}\Psi(p_2^*)], \tag{17}$$

$$\mathcal{M}_d^{*\rho} = i\frac{\Gamma_{\rho NN}g_{\rho N\Delta}I_d}{m_\rho}[\bar{\Psi}(p_3^*)\gamma_\mu\Psi(p_1^*)]\times\frac{g^{\mu\tau}-Q_d^{*\mu}Q_d^{*\tau}/m_\rho^2}{Q_d^{*2}-m_\rho^2} \times[\bar{\Delta}_\sigma(p_4^*)\gamma_\lambda\gamma_5(Q_d^{*\lambda}\delta_{\sigma\tau}-Q_d^{*\sigma}\delta_{\lambda\tau})\Psi(p_2^*)]. \tag{18}$$

The upper index in $\mathcal{M}_{d,e}^{*\text{meson}}$ refers to the exchanged boson, and the lower index to the direct or exchange process. $Q_d^{*\mu}=p_3^{*\mu}-p_1^{*\mu}$ for the direct term; the exchange term $\mathcal{M}_e^*$ is obtained by $p_1^{*\mu}\longleftrightarrow p_2^{*\mu}$ and $Q_e^{*\mu}=p_3^{*\mu}-p_2^{*\mu}$. The isospin factors I_d and I_e can be found in the Ref. [24].

The in-medium $NN\to N\Delta$ cross section is the in-medium elementary two-body cross section averaged over the mass of Δ by considering the Δ as the short-living resonance, and it can be written as

$$\sigma^*_{NN\to N\Delta} = \int_{m^*_{\Delta,\min}}^{m^*_{\Delta,\max}} \mathrm{d}m^*_\Delta f(m^*_\Delta)\tilde{\sigma}^*(m^*_\Delta), \tag{19}$$

$\tilde{\sigma}^*(m^*_\Delta)$ is the in-medium elementary two-body cross section. In the center-of-mass frame of colliding nucleons, it is obtained as

$$\begin{aligned}\tilde{\sigma}^*(m^*_\Delta) &= \frac{1}{4F^*}\int\frac{d^3\boldsymbol{p}_3^*}{(2\pi)^3 2E_3^*}\frac{d^3\boldsymbol{p}_4^*}{(2\pi)^3 2E_4^*} \times(2\pi)^4\delta^4(p_1+p_2-p_3-p_4)\overline{|\mathcal{M}^*|^2} \\ &= \frac{1}{64\pi^2}\int\frac{|\boldsymbol{p}^*_{\text{out,c.m.}}|}{\sqrt{s^*_{\text{in}}}\sqrt{s^*_{\text{out}}}|\boldsymbol{p}^*_{\text{in,c.m.}}|}\overline{|\mathcal{M}^*|^2}\mathrm{d}\Omega,\end{aligned} \tag{20}$$

where $\boldsymbol{p}^*_{\text{in,c.m.}}$ and $\boldsymbol{p}^*_{\text{out,c.m.}}$ are the momenta of incoming (1 and 2) and outgoing particles (3 and 4), respectively. $F^*=\sqrt{(p_1^*p_2^*)^2-p_1^{*2}p_2^{*2}}=\sqrt{s^*_{\text{in}}}|\boldsymbol{p}^*_{\text{in,c.m.}}|$ is the invariant flux factor, $s^*_{\text{in}}=(p_1^*+p_2^*)^2$, and $s^*_{\text{out}}=(p_3^*+p_4^*)^2$. Here $\overline{|\mathcal{M}^*|^2}=\dfrac{1}{(2s_1+1)(2s_2+1)}\sum_{s_1s_2s_3s_4}|\mathcal{M}^*|^2$ is,

$$\begin{aligned}\sum_{s_1s_2s_3s_4}|\mathcal{M}^*|^2 = \sum_{s_1s_2s_3s_4}\{&|\mathcal{M}_d^{*\pi}|^2-\mathcal{M}_d^{*\pi\dagger}\mathcal{M}_e^{*\pi}-\mathcal{M}_e^{*\pi\dagger}\mathcal{M}_d^{*\pi}+|\mathcal{M}_e^{*\pi}|^2 \\ &+|\mathcal{M}_d^{*\rho}|^2-\mathcal{M}_d^{*\rho\dagger}\mathcal{M}_e^{*\rho}-\mathcal{M}_e^{*\rho\dagger}\mathcal{M}_d^{*\rho}+|\mathcal{M}_e^{*\rho}|^2 \\ &+\mathcal{M}_d^{*\pi\dagger}\mathcal{M}_d^{*\rho}-\mathcal{M}_d^{*\pi\dagger}\mathcal{M}_e^{*\rho}-\mathcal{M}_e^{*\pi\dagger}\mathcal{M}_d^{*\rho}+\mathcal{M}_e^{*\pi\dagger}\mathcal{M}_e^{*\rho} \\ &+\mathcal{M}_d^{*\rho\dagger}\mathcal{M}_d^{*\pi}-\mathcal{M}_d^{*\rho\dagger}\mathcal{M}_e^{*\pi}-\mathcal{M}_e^{*\rho\dagger}\mathcal{M}_d^{*\pi}+\mathcal{M}_e^{*\rho\dagger}\mathcal{M}_e^{*\pi}\}.\end{aligned} \tag{21}$$

All the terms are calculated by using Mathematics with the packages of "High Energy Physics" [37]. Here, we only show the direct term as an example for π mesons, i.e., $\sum_{s_1s_2s_3s_4}|\mathcal{M}_d^{*\pi}|^2$:

$$\begin{aligned}\sum_{s_1s_2s_3s_4}|\mathcal{M}_d^{*\pi}|^2 &= \left(\frac{g_{\pi NN}g_{\pi N\Delta}I_d}{m_\pi^2(Q_d^{*2}-m_\pi^2)}\right)^2 \\ &\times\sum_{s_1s_2s_3s_4}[\Psi(p_1^*)\bar{\Psi}(p_1^*)\gamma_\mu\gamma_5 Q_d^{*\mu}\Psi(p_3^*)\bar{\Psi}(p_3^*)\gamma_\sigma\gamma_5 Q_d^{*\sigma}] \\ &\times[\Psi(p_2^*)\bar{\Psi}(p_2^*)Q_d^{*\nu}\Delta_\nu(p_4^*)\bar{\Delta}_\tau(p_4^*)Q_d^{*\tau}] \\ &= \left(\frac{g_{\pi NN}g_{\pi N\Delta}I_d}{m_\pi^2(t^*-m_\pi^2)}\right)^2 \\ &\times\frac{2(m^*_{N_1}+m^*_{N_3})^2((m^*_{N_1}-m^*_{N_3})^2-t^*)}{3m^{*2}_{\Delta_4}} \\ &\times\left((m^*_{\Delta_4}-m^*_{N_2})^2-t^*\right)\left((m^*_{N_2}+m^*_{\Delta_4})^2-t^*\right)^2\end{aligned} \tag{22}$$

where $t=Q_d^{*2}$ for $|\mathcal{M}_e^{*\pi}|^2$ is $N_1\leftrightarrow N_2$. In Eq. (20), note that the crucial requirement for two-body collisions is the energy-momentum conservation in terms of incoming and outgoing canonical momenta $(p^\mu_{1,2},\ p^\mu_{3,4})$, i.e., $\delta^4(p_1+p_2-p_3-p_4)$. From the viewpoint of kinetic momentum, the energy-momentum conservation $p_1^\mu+p_2^\mu=p_3^\mu+p_4^\mu$ can be expressed as $p_1^{*\mu}+\Sigma_1^{*\mu}+p_2^{*\mu}+\Sigma_2^{*\mu}=p_3^{*\mu}+\Sigma_3^{*\mu}+p_4^{*\mu}+\Sigma_4^{*\mu}$, and $p_1^{*\mu}+p_2^{*\mu}=p_3^{*\mu}+p_4^{*\mu}-\Delta\Sigma^\mu$, where, $\Delta\Sigma^\mu=\Sigma_1^\mu+\Sigma_2^\mu-\Sigma_3^\mu-\Sigma_4^\mu$ is the change in kinetic momentum between the initial and final states. The change in effective energy is expressed as $\Delta\Sigma^0=\Sigma_1^0+\Sigma_2^0-\Sigma_3^0-\Sigma_4^0$, which is the same as the equation in Ref. [38]. A similar issue exists in the calculation of $m^*_{\min}$, $m^*_{\max}$ and $\Gamma(m^*_\Delta)$ which are described in the following.

$m^*_{\Delta,\min}$, in the equation of the cross section, is determined by the $\Delta\to N+\pi$ in isospin asymmetric nuclear matter as in Refs. [22, 23], when both N and π are at rest; the modification of scalar and vector self-energies in this isospin exchange process should also be considered. Thus, $m^*_{\Delta,\min}=m^*_N+\Sigma^0_N+m^*_\pi+\Pi_P(\omega,\boldsymbol{q})-\Sigma^0_\Delta=m^*_N+m^*_\pi-\Delta\Sigma^0_d$, with $\Delta\Sigma^0_d=\Sigma^0_N+\Pi_P(\omega,\boldsymbol{q})-\Sigma^0_\Delta$. Considering m^*_π/m_π less than ~10% at normal density from the calculations by Kaiser and Weise [39], we assume that the effect of the nuclear mean field on the pions is negligible and $m^*_\pi=m_\pi$. Thus, we have $\Delta\Sigma^0_d=\Sigma^0_\Delta-\Sigma^0_N$. $m^*_{\Delta,\max}$ is evaluated from $NN\to\Delta N$ for producing N and Δ at rest:

$$m^*_{\Delta,\max}=\sqrt{s}-m^*_{N_3}-\Sigma^0_{N_3}-\Sigma^0_{\Delta_4}. \tag{23}$$

The in-medium Δ mass distribution $f(m^*_\Delta)$ is another important factor of in-medium $NN\to N\Delta$ cross section for which proper energy conservation is required, because $f(m^*_\Delta)$ is related to the $\Delta\to N+\pi$ process in isospin asymmetric nuclear matter. In this study, the spectral function of Δ is taken as in Ref. [27],

$$f(m^*_\Delta)=\frac{2}{\pi}\frac{m^{*2}_\Delta\Gamma(m^*_\Delta)}{(m^{*2}_{0,\Delta}-m^{*2}_\Delta)^2+m^{*2}_\Delta\Gamma^2(m^*_\Delta)}. \tag{24}$$

Here, $m^*_{0,\Delta}$ is the effective pole mass of Δ, and $\dfrac{2}{\pi}$ is the normalization factor. The decay width $\Gamma(m^*_\Delta)$ is taken in

the parametric form [27]

$$\Gamma(m^*_\Delta)=\Gamma_0\frac{q^3(m^*_\Delta,m^*_N,m^*_\pi)}{q^3(m^*_{0,\Delta},m^*_N,m^*_\pi)}\times\frac{q^3(m^*_{0,\Delta},m^*_N,m^*_\pi)+\eta^2}{q^3(m^*_\Delta,m^*_N,m^*_\pi)+\eta^2}\frac{m^*_{0,\Delta}}{m^*_\Delta}, \tag{25}$$

where

$$q(m^*_\Delta,m^*_N,m^*_\pi)=\sqrt{\frac{\left((m^*_\Delta+\Sigma^0_\Delta-\Sigma^0_N)^2+m^{*2}_N-m^{*2}_\pi\right)^2}{4(m^*_\Delta+\Sigma^0_\Delta-\Sigma^0_N)^2}-m^{*2}_N} \tag{26}$$

is the center-of-mass momentum of nucleon and pion from the decay of Δ in its rest frame. The factor of $(m^*_\Delta+\Sigma^0_\Delta-\Sigma^0_N)$ in Eq. (26) comes from properly considering the energy conservation in $\Delta\to N\pi$ process in the isospin asymmetric nuclear matter. The coefficients of Γ_0=0.118 GeV and η= 0.2 GeV/c are used in the above parametrization formula.

As an example, we present the decay width $\Gamma(m^*_\Delta)$ and $f(m^*_\Delta)$ as a function of $m^*_\Delta-m^*_{\Delta,\min}$ in Fig. 3 for symmetric nuclear matter $I=0$ and $\rho_B=\rho_0$ because their dependence on isospin asymmetry and density is negligible. $m^*_\Delta-m^*_{\Delta,\min}$ is used in the plot of the $\Gamma(m^*_\Delta)$ and $f(m^*_\Delta)$ because the $m^*_{\Delta,\min}$ are different in different parameter sets, such as NL$\rho\delta$-Δ (black lines), DDMEδ-Δ (red lines), and DDRH$\rho\delta$-Δ (green lines). Based on Eq. (26), the values of m^*_Δ can be related to the momentum of nucleon and pion from the decay of Δ in its rest frame. The larger the m^*_Δ is, the larger the q is.

The form factors are adopted to effectively consider the contribution from high-order terms and the finite size of baryons [24, 40], which read

$$F_N(t^*)=\frac{\Lambda_N^2}{\Lambda_N^2-t^*}\exp\left(-b\sqrt{s^*-4m^{*2}_N}\right), \tag{27}$$

$$F_\Delta(t^*)=\frac{\Lambda_\Delta^2}{\Lambda_\Delta^2-t^*}. \tag{28}$$

Here, $F_N(t^*)$ is the form factor for nucleon-meson-nucleon , $F_\Delta(t^*)$ is the form factor for nucleon-meson-Δ coupling, and b=0.046 GeV^{-1} for both ρNN and πNN. The cutoff parameter $\Lambda_{\pi NN}\approx 1$ GeV for all selected three parameter sets, i.e., NL$\rho\delta$, DDMEδ, and DDRH$\rho\delta$. $\Lambda_{\rho NN}$ and $\Lambda_{\pi N\Delta}$ are determined by best fitting the data of $NN\to N\Delta$ cross section in free space [41] ranging from $\sqrt{s}$=2.0 to 5.0 GeV. In Table 1, $\Lambda_{\rho N\Delta}$ is determined based on the relationship $\Lambda_{\rho N\Delta}=\Lambda_{\rho NN}\frac{\Lambda_{\pi N\Delta}}{\Lambda_{\pi NN}}$ as in [24].

3 Results and discussions

3.1 Cross section and its medium correction

Figure 4(a) shows the calculated $\sigma^*_{pp\to n\Delta^{++}}$ as a function of Q, and 4(b) shows $\frac{d\sigma^*}{d\cos\theta}$at the beam energy of 0.97 GeV in free space. Q represents the kinetic energy above the pion production threshold energy $\sqrt{s_{\rm th}}=m^*_{N_3}+m^*_{\Delta,\min}+\Sigma^0_{N_3}+\Sigma^0_\Delta$, which is defined as

$$\begin{aligned}Q=&\sqrt{s_{\rm in}}-\sqrt{s_{\rm th}}=E^*_{N_1}+E^*_{N_2}+\Sigma^0_{N_1}+\Sigma^0_{N_2}\\&-m^*_{N_3}-m^*_{\Delta,\min}-\Sigma^0_{N_3}-\Sigma^0_\Delta\simeq(E^*_{N_1}-m^*_{N_1})\\&+(E^*_{N_2}-m^*_{N_2});+m_{N_1}+m_{N_2}-m_{N_3}-m_{\Delta,\min}\\&+\Delta\Sigma^S+\Delta\Sigma^0,\end{aligned} \tag{29}$$

where $\Delta\Sigma^S=\Sigma^S_{N_1}+\Sigma^S_{N_2}-\Sigma^S_{N_3}-\Sigma^S_\Delta$. The black circles and squares correspond to the experimental data [41, 42]. The black solid line, dashed lines, and dotted lines are the results for NL$\rho\delta$-Δ, DDMEδ-Δ, and DDRH$\rho\delta$-Δ, respectively. To investigate the impacts of different effective Lagrangian parameter sets on the in-medium $NN\to N\Delta$ cross section, all the selected parameter sets are adjusted to reproduce the experimental data of $NN\to N\Delta$ cross sections and their differential cross sections at E_b =0.97 GeV, where the data of differential cross section can be obtained.

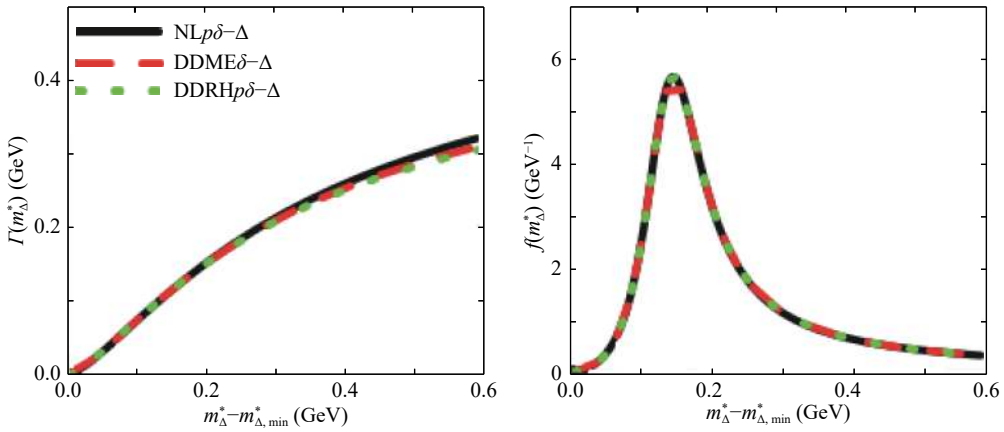

Fig. 3. (color online) (a) $\Gamma(m^*_\Delta)$ and (b) $f(m^*_\Delta)$ as a function of $m^*_\Delta-m^*_{\Delta,\min}$ at $\rho_B=\rho_0$ for symmetric nuclear matter $I=0$. The black, red, and green lines are the results for NL$\rho\delta$-Δ, DDMEδ-Δ and DDRH$\rho\delta$-Δ, respectively.

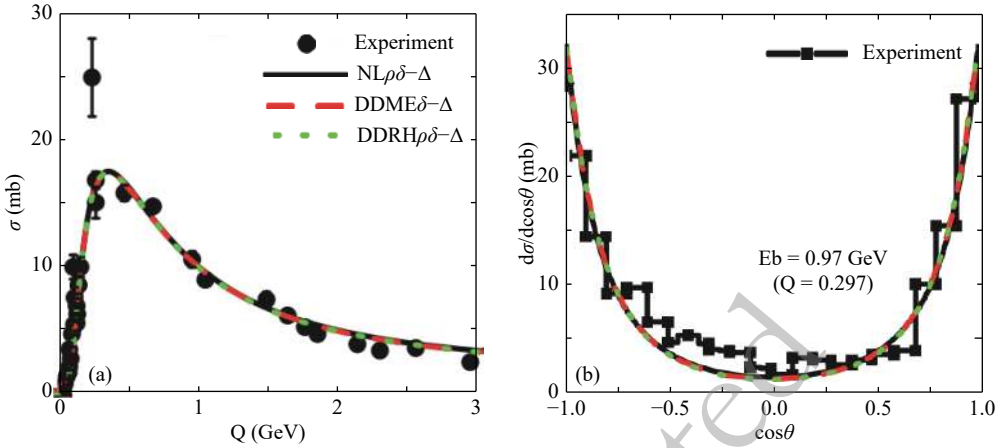

Fig. 4. (color online) (a) $\sigma^*_{pp\to n\Delta^{++}}$ as a function of Q for for NL$\rho\delta$-Δ, DDMEδ-Δ and DDRH$\rho\delta$-Δ in free space , the experimental data are from [41]; (b) $\frac{d\sigma}{d\cos\theta}$ as a function of $\cos\theta$ at beam energy $E_b = 0.97$ GeV, the experimental data from [42]. The lines with different colors correspond to different parameter sets.

Figures 5(a) and (b) present the results of $\sigma^*_{pp\to n\Delta^{++}}$ at ρ_0 and $2\rho_0$ in symmetric nuclear matter for different parameter sets, respectively. The black solid line, red dashed lines, and green dotted lines are the results for NL$\rho\delta$-Δ, DDMEδ-Δ, and DDRH$\rho\delta$-Δ, respectively. The values of $\sigma^*_{pp\to n\Delta^{++}}$ depend on the selected parameter sets. The NL$\rho\delta$-Δ predicts the largest in-medium $NN\to N\Delta$ cross section among the three parameter sets, and $\sigma^*_{\mathrm{NL}\rho\delta-\Delta} > \sigma^*_{\mathrm{DDME}\delta-\Delta} > \sigma^*_{\mathrm{DDRH}\rho\delta-\Delta}$, especially at $2\rho_0$. The difference between $\sigma^*_{\mathrm{DDME}\delta-\Delta}$ and $\sigma^*_{\mathrm{DDRH}\rho\delta-\Delta}$ is comparatively small owing to the slight difference between the effective masses as shown in Table 1. This can be understood from the equation of in-medium $NN\to N\Delta$ cross sections, such as Eq. (22), where the values of cross section monotonically increase with the effective mass of the nucleon and Δ. The larger the effective mass, the larger the cross section. Similar to the symmetric nuclear matter, the in-medium $NN\to N\Delta$ cross sections in isospin asymmetric nuclear matter also has $\sigma^*_{\mathrm{NL}\rho\delta-\Delta} > \sigma^*_{\mathrm{DDME}\delta-\Delta} > \sigma^*_{\mathrm{DDRH}\rho\delta-\Delta}$. This can be observed in Fig. 5(c)-(f), where $\sigma^*_{pp\to n\Delta^{++}}$ and $\sigma^*_{nn\to p\Delta^-}$ at ρ_0 (left panels) and $2\rho_0$ (right panels) for isospin asymmetry $I = 0.2$ are shown examples.

Based on our discussion in [23], the in-medium $NN\to N\Delta$ cross section is split in isospin asymmetric nuclear matter owing to the effective mass splitting for nucleons and Δs. The values of in-medium cross sections of $pp\to n\Delta^{++}$, $pp\to p\Delta^{+}$, $pn\to n\Delta^{+}$, $pn\to p\Delta^{0}$, $nn\to n\Delta^{0}$, and $nn\to p\Delta^{-}$ do not satisfy the Clebsch-Gordan coefficients as in free space. This can be understood from the expression of matrix element in Eq. (22). For example, if there is no isospin splitting for nucleon and Δ effective mass, the difference of $|\mathcal{M}|^2$ between the different channels is due to I_d^2 or I_e^2 because the terms contains m_N^*, m_Δ^*, and t^* in $|\mathcal{M}|^2$ have the same contributions to different channels. However, in the isospin asymmetric nuclear matter, there is isospin splitting on the nucleon and Δ effective mass, and it causes different values of m_N^*, m_Δ^*, and t^* in $|\mathcal{M}|^2$, in addition to I_d^2 and I_e^2 for different channels.

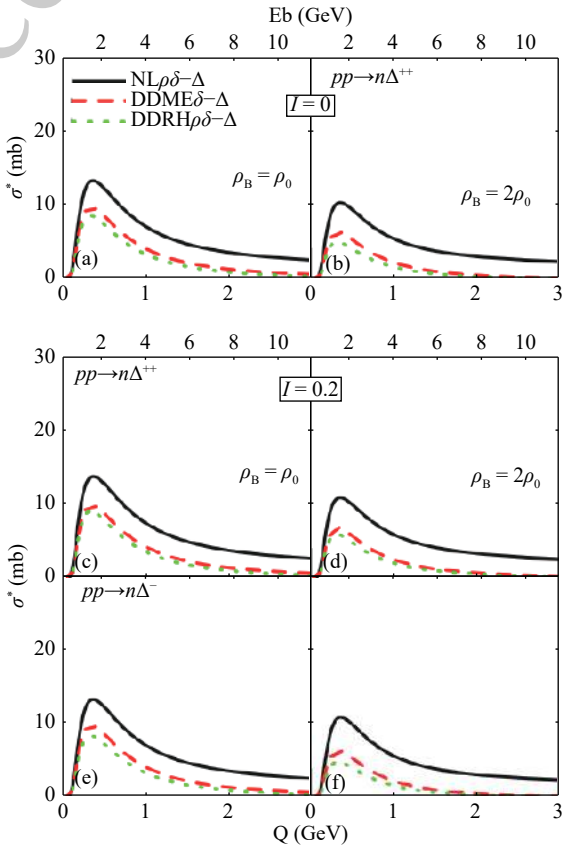

Fig. 5. (color online) $\sigma^*_{NN\to N\Delta}$ as a function of Q, (a) and (b) for symmetric nuclear matter $I = 0$; (c)-(f) for asymmetric nuclear I=0.2.

In the left panels of Fig. 6, we present the R ratios in the symmetric nuclear matter. The upper, middle, and

bottom panels correspond to the results for different beam energies or E_b= 0.4 (Q =0.052 GeV), 0.8 (Q = 0.227 GeV), and 1.2 GeV (Q= 0.389 GeV), respectively. The different channels have the same in-medium correction factor R, and their values decrease with the increase in density. This is consistent with the results of [19, 27]. Similar to the dependence of cross section on the parameter sets, $R_{\mathrm{NL}\rho\delta-\Delta} > R_{\mathrm{DDME}\delta-\Delta} > R_{\mathrm{DDRH}\rho\delta-\Delta}$.

For isospin asymmetric nuclear medium, in the right panels of Fig. 6, the R ratios obtained with the selected parameter sets also decrease as functions of density, and they are split according to the different isospin states of collision channels. Near the threshold energy, the R values clearly depend on the channel of $NN \to N\Delta$ and $R(pp \to n\Delta^{++}) > R(Np \to N\Delta^{+}) > R(Nn \to N\Delta^{0}) > R(nn \to p\Delta^{-})$, here $N = n$ or p. The amplitude of the splitting mainly attributes to the effective mass splitting of nucleon and Δ, which are presented in Table 1, via the effective mass changes between the incoming and outgoing particles, i.e., $\Delta\Sigma^S$, and the effective energy changes, i.e., $\Delta\Sigma^0$ for different channels. In the calculation of the in-medium $NN \to N\Delta$ cross section, the values of $\Delta\Sigma^S$ and $\Delta\Sigma^0$ provide the opposite contribution on their isospin effects through Q. Near the threshold ($E_b \approx$0.4 GeV), the R values are mainly effected by the effective mass changes $\Delta\Sigma^S$ and effective energy changes $\Delta\Sigma^0$. When the beam energy increases up to 0.8 GeV, the splitting of R among the different channels of $NN \to N\Delta$ tends to vanish because the contributions from scalar and vector self-energies become relatively smaller than the contributions of kinetic energy.

Near the threshold energy, the splitting of R is larger in NL$\rho\delta$-Δ than that in DDRH$\rho\delta$-Δ and DDMEδ-Δ owing to the stronger nucleons and Δs effective mass splitting in NL$\rho\delta$-Δ. The splitting of R for different channels vanishes when $E_b >$ 0.8 GeV for all parameter sets; however, the reduction of in-medium correction follows $R_{\mathrm{NL}\rho\delta-\Delta} > R_{\mathrm{DDME}\delta-\Delta} > R_{\mathrm{DDRH}\rho\delta-\Delta}$, which is caused by the decrease of effective masses for the three parameter sets in Table 1. This can clearly be seen in Fig. 7, in which $R(2\rho_0)$ increases with an increase in m_N^*/m_N (or L). This suggests that adjusting the medium correction factor R in transport models should also simultaneously consider the stiffness of isospin asymmetric nuclear EOS. However, the concrete relationship between the medium correction factor and stiffness of symmetry energy still needs to be investigated, for example, by analyzing the various proposed RMF parameters.

Because the differential $NN \to N\Delta$ cross section determines the scattering angle for colliding particles in transport models, the medium effects on the differential cross sections for $NN \to N\Delta$ should be discussed. A parametrized form of differential cross sections from experimental data [43] is usually used in various codes without considering the medium correction effects. Recently, Wang et al. [44] tried to understand the influence of the

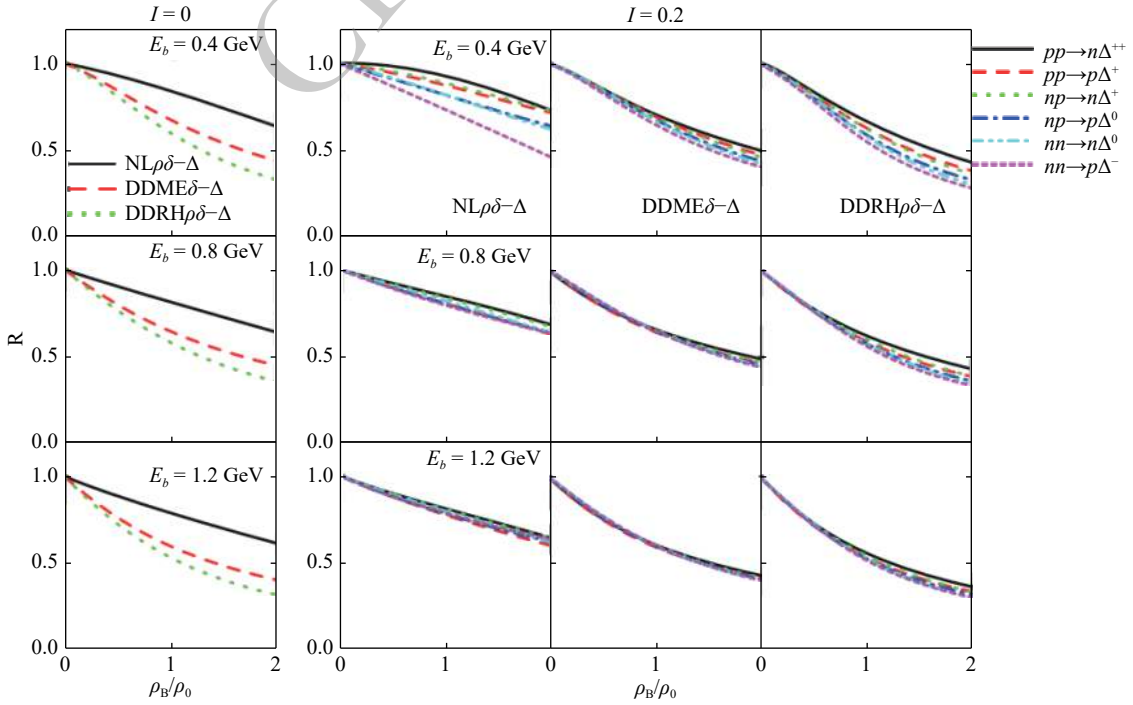

Fig. 6. (color online) Medium correction factor $R = \sigma^*/\sigma^{\mathrm{free}}$ of different channels (with different color) as the function of density for E_b= 0.4, 0.8, and 1.2 GeV (Q= 0.052, 0.227, and 0.389 GeV) for different parameter sets. Left three panels are for symmetric nuclear matter (I= 0), right nine panels for asymmetric nuclear matter (I=0.2).

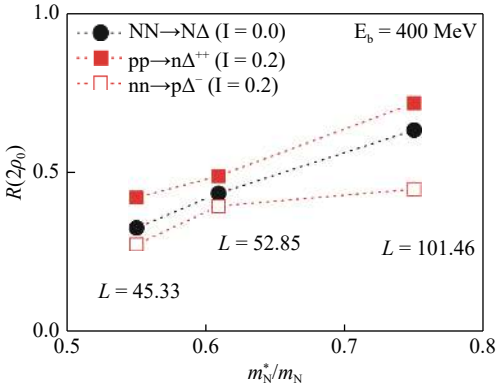

Fig. 7. (color online) Medium correction factor R at $\rho_B = 2\rho_0$ in E_b =0.4 GeV for different parameter sets, i.e., NL$\rho\delta$-Δ, DDRH$\rho\delta$-Δ and DDMEδ-Δ, the unit of L is MeV.

different forms of differential cross sections on the elliptical flow in the ultrarelativistic quantum molecular dynamics model simulations; their results show that it could influence nuclear stopping power, and direct and elliptic flow at high beam energies. It also stimulated the theoretical understanding of the in-medium differential $NN \to N\Delta$ cross sections, which are necessary for developing isospin-dependent transport codes. The in-medium differential cross sections become more isotropic with an increase in density for elastic NN collisions [12]; similar behavior was observed in the $NN \to N\Delta$ differential cross section in symmetric nuclear matter [27]. Our calculations also confirm the conclusion that the differential cross section for $NN \to N\Delta$ tends to be more isotropic for all the parameter sets we used for the symmetric nuclear medium, especially at the twice normal density near the threshold energy. Furthermore, the same behavior of the in-medium $NN \to N\Delta$ differential cross sections can be observed in asymmetric matter. As shown in Fig. 8, we present the results of $pp \to n\Delta^{++}$ and $nn \to p\Delta^{-}$ channels at $E_b = 0.4$ GeV as an example. The medium correction of the differential cross sections is strong, and it mainly appears at the forward and backward regions, i.e., $\theta_{c.m.} < 60°$ and $\theta_{c.m.} > 120°$, respectively. When the beam energy is higher, the medium correction effects become weaker at approximately $\theta_{c.m.} = 90°$; however, it still exists at forward and backward regions.

4 Summary

In summary, we studied the in-medium $NN \to N\Delta$ integrate and differential cross sections in isospin asymmetric nuclear medium within the one-boson exchange model. Three different interaction parameter sets, with ρ and δ mesons, were adopted in this work. Our calculations show that $\sigma^*_{NN\to N\Delta}$ decreases with the an increase in the density; the in-medium differential cross sections becomes more isotropic with an increase in the density near

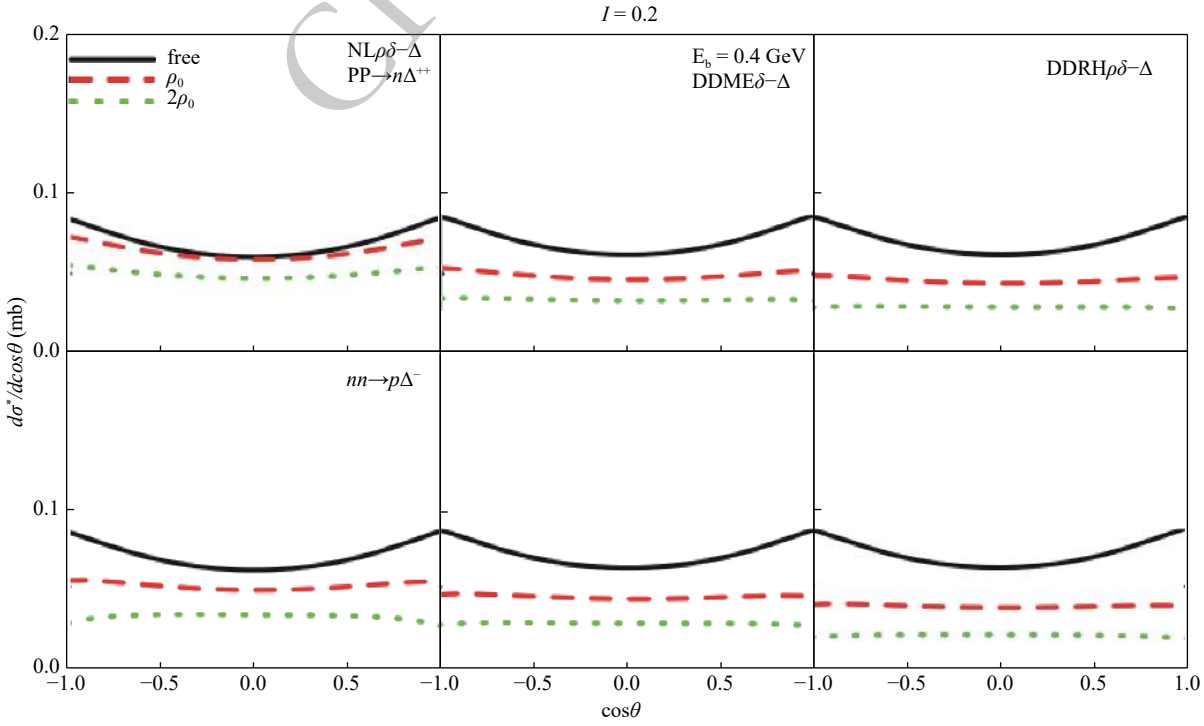

Fig. 8. (color online) $d\sigma^*/d\cos\theta$ for $pp \to n\Delta^{++}$ and $nn \to p\Delta^{-}$ channels as a function of $\cos\theta$ at the beam energy of 0.4 GeV. The lines with different colors correspond to $\rho_B = 0, \rho_0, 2\rho_0$ in asymmetric nuclear matter (I=0.2). The panels from left to right refer to the results obtained with NL$\rho\delta$-Δ, DDMEδ-Δ, and DDHR$\rho\delta$-Δ.

the threshold energy for all selected parameter sets. At the given density, the medium correction factor R decreases with a decrease in the effective mass, or with a decrease in the slope of symmetry energy. This trend can be used to mimic the deficiency of transport models, where the mean field and in-medium nucleon-nucleon cross section are adjusted separately to fit the data. By considering the relationship between the in-medium $NN \to N\Delta$ cross sections and slope of symmetry energy in the transport model calculations, it could reduce the ambiguity of the constrains on either EOS or in-medium $NN \to N\Delta$ cross section through the comparison with HIC data.

To concrete the relationship between the EOS and in-medium $NN \to N\Delta$ cross section, further analysis on the proposed RMF parameter sets are required. For example, there are 263 RMF parameter sets [35] and most of them only include σ, ω, and ρ mesons. In parameter sets with σ, ω, and ρ mesons, the relation obtained in this study can be modified because the isospin splitting of R is only caused by the isospin splitting of effective energy by the ρ meson. Further study in this field will be interesting and helpful for reliable extraction of the EOS or in-medium NN cross section through transport models.

References

1 Chen Liewen, Zhang Fengshou, Zeng Xianghua, and Jin Genming, Chin. Phys. C, **22**: 1035 (1998)
2 J.-Y. Liu, W.-J. Guo, S.-J. Wang, W. Zuo, Q. Zhao, and Y.-F. Yang, Phys. Rev. Lett., **86**: 975 (2001)
3 Qingfeng Li and Zhuxia Li, Chin. Phys. Lett., **19**: 321 (2002)
4 Y. X. Zhang and Z. X. Li, Phys. Rev. C, **74**: 014602 (2006)
5 G. Lehaut, D. Durand, O. Lopez, E. Vient, A. Chbihi, J. D. Frankland, E. Bonnet, B. Borderie, R. Bougault, E. Galichet, D. Guinet, Ph. Lautesse, N. Le Neindre, P. Napolitani, M. Parlog, M. F. Rivet, and E. Rosato, Phys. Rev. Lett., **104**: 232701 (2010)
6 O. Lopez, D. Durand, G. Lehaut, B. Borderie, J. D. Frankland, M. F. Rivet, R. Bougault, A. Chbihi, E. Galichet, D. Guinet, M. La Commara, N. Le Neindre, I. Lombardo, L. Manduci, P. Marini, P. Napolitani, M. Parlog, E. Rosato, G. Spadaccini, E. Vient, and M. Vigilante (INDRA Collaboration), Phys. Rev. C, **90**: 064602 (2014)
7 L.-W. Chen, F.-S. Zhang, and Z.-Y. Zhu, Phys. Rev. C, **61**: 067601 (2000)
8 Y. J. Wang, C. C. Guo, Q. F. Li, Z. X. Li, J. Su, and H. F. Zhang, Phys. Rev. C, **94**: 024608 (2016)
9 G. Q. Li and R. Machleidt, Phys. Rev. C, **48**: 1702 (1993)
10 Y.H. Cai, H.Q. Song, and U. Lombardo, Chin. Phys. Lett., **13**: 6 (1996)
11 Qingfeng Li, Zhuxia Li, and Guangjun Mao, Phys. Rev. C, **62**: 014606 (2000)
12 H. F. Zhang, U. Lombardo, and W. Zuo, Phys. Rev. C, **82**: 015805 (2010)
13 D. Persram and C. Gale, Phys. Rev. C, **65**: 064611 (2002)
14 B.-A. Li and L.-W. Chen, Phys. Rev. C, **72**: 064611 (2005)
15 Zhao-Qing Feng, Phys. Rev. C, **85**: 014604 (2012)
16 Yingxun Zhang, Zhuxia Li, and Pawel Danielewicz, Phys. Rev. C, **75**: 034615 (2007)
17 Pengcheng Li, Yongjia Wang, Qingfeng Li, Chenchen Guo, and Hongfei Zhang, Phys. Rev. C, **97**: 044620 (2018)
18 Pawel Danielewicz, Nucl. Phys. A, **673**: 357 (2000)
19 Q. Li and Z. Li, Phys. Lett. B, **773**: 557 (2017)
20 T. Song and C. M. Ko, Phys. Rev. C, **91**: 014901 (2015)
21 G. Ferini, M. Colonna, T. Gaitanos, and M. D. Toro, Nucl. Phys. A, **762**: 147 (2005)
22 Z. Zhang and C. M. Ko, Phys. Rev. C, **95**: 064604 (2017)
23 Ying Cui, Yingxun Zhang, and Zhuxia Li, Phys. Rev. C, **98**: 054605 (2018)
24 S. Huber and J. Aichelin, Nucl. Phys. A, **573**: 587 (1994)
25 R. Machleidt, K. Holinde, and C. Elster, Phys. Rep., **149**: 1 (1987)
26 M. Benmerrouche, R. M. Davidson, and N. C. Mukhopadhyay, Phys. Rev. C, **39**: 2339 (1989)
27 A. Larionov and U. Mosel, Nucl. Phys. A, **728**: 135 (2003)
28 V. Dmitriev, O. Sushkov, and C. Gaarde, Nucl. Phys. A, **459**: 503 (1986)
29 A. Engel, Diplomarbeit, Giessen (1990)
30 F. Hofmann, C. M. Keil, and H. Lenske, Phys. Rev. C, **64**: 034314 (2001)
31 B. Liu, V. Greco, V. Baran, M. Colonna, and M. Di Toro, Phys. Rev. C, **65**: 045201 (2002)
32 T. Gaitanos, M. Di Toro, S. Typel, V. Baran, C. Fuchs, V. Greco, and H. H. Wolter, Nucl. Phys. A, **732**: 24 (2004)
33 P. Gögelein, E. N. E. van Dalen, C. Fuchs, and H. Müther, Phys. Rev. C, **77**: 025802 (2008)
34 X. Roca-Maza, X. Viñas M. Centelles, P. Ring, and P. Schuck, Phys. Rev. C, **84**: 054309 (2011)
35 M. Dutra, O. Lourenço, S. S. Avancini, B. V. Carlson, A. Delfino, D. P. Menezes, C. Providência, S. Typel, and J. R. Stone, Phys. Rev. C, **90**: 055203 (2014)
36 G. Baym ans S. A. Chin, Nucl. Phys. A, **262**: 527 (1976)
37 http://www.feyncalc.org.
38 Zhen Zhang and Che Ming Ko, Phys. Rev. C, **97**: 014610 (2018)
39 N. Kaiser and W. Weise, Phys. Lett. B, **512**: 283 (2001)
40 T. Vetter, A. Engel, T. Bir, and U. Mosel, Phys. Lett. B, **263**: 153 (1991)
41 A. Baldini, V. Flaminio, W. G. Moorhead, and D. R. O. Morrison, *Total Cross-Sections for Reactions of High Energy Particles*, edited by H. Schopper, Landolt-Börnstein, Vol. 12, Pt. B (Springer-Verlag, Berlin, 1987)
42 D.V. Bugg et al, Phys. Rev., **133**: B1017 (1964)
43 J. Cugnon, D. LHote, and J. Vandermeulen, Nucl. Instrum. Methods Phys. Res., Sect. B, **111**: 215 (1996)
44 Yongjia Wang, Chenchen Guo, Qingfeng Li, Zhuxia Li, Jun Su, and Hongfei Zhang, Phys. Rev. C, **94**: 024608 (2016)